



# CHORUS

This is the accepted manuscript made available via CHORUS. The article has been published as:

## Stacking fault energies of nondilute binary alloys using special quasirandom structures

Jonas L. Kaufman, Gregory S. Pomrehn, Aurora Pribram-Jones, Reza Mahjoub, Michael Ferry, Kevin J. Laws, and Lori Bassman

Phys. Rev. B **95**, 094112 — Published 14 March 2017

DOI: [10.1103/PhysRevB.95.094112](https://doi.org/10.1103/PhysRevB.95.094112)

# Stacking fault energies of non-dilute binary alloys using special quasirandom structures

Jonas L. Kaufman,<sup>1</sup> Gregory S. Pomrehn,<sup>2</sup> Aurora Pribram-Jones,<sup>3,4</sup>  
Reza Mahjoub,<sup>5</sup> Michael Ferry,<sup>5</sup> Kevin J. Laws,<sup>5</sup> and Lori Bassman<sup>1</sup>

<sup>1</sup>*Harvey Mudd College, Claremont, CA 91711, USA*

<sup>2</sup>*The Boeing Company, Seattle, WA 98108, USA*

<sup>3</sup>*Lawrence Livermore National Laboratory, Livermore, CA 94550, USA*

<sup>4</sup>*Department of Chemistry, University of California, Berkeley, CA 94720 USA*

<sup>5</sup>*School of Materials Science and Engineering, UNSW Australia, Sydney, NSW 2052, Australia*

(Dated: February 21, 2017)

Generalized stacking fault energies of non-dilute binary alloys in the Ag-Au-Pd system are calculated using density functional theory and special quasirandom structures. Supercells containing 90 and 135 atoms are compared for direct calculations of the generalized stacking fault energy, and the axial interaction model is used to estimate the intrinsic stacking fault energy. The axial interaction model approximates the directly calculated energy to within 10% in most cases, but is sensitive to the particular structures used. Increasing the number of atoms used for direct calculations decreases the uncertainty of the calculated stacking fault energies in most cases, and we show that this uncertainty is related to certain correlations between pairs of adjacent layers within the supercell.

## I. INTRODUCTION

Ductility is a key consideration for materials in many engineering applications and their respective processing routes. Bulk or macroscopic ductility in metallic materials is a direct result of which deformation modes or mechanisms are accessible for a particular crystalline lattice. For face-centered cubic (fcc) metals (such as Al, Cu, Ni, Ag, Au and their alloys) where dislocation glide is the dominant means of accommodating strain, primary dislocations are essentially split into two (Shockley) partial dislocations as a means of lowering the structural energy of the crystal lattice with respect to the existence of a dynamic dislocation<sup>1</sup>. The existence of these partial dislocations creates a fault in the stacking sequence of the fcc lattice, changing the crystal structure locally. When the path of these two partial dislocations is hindered, e.g. by a crystal flaw or grain boundary, these two partial dislocations must recombine in order to cross slip around the hindrance. The ease by which these partial dislocations can be recombined to enable cross slip and continue to accommodate strain is directly related to the energy associated with the stacking fault created by the two partial dislocations i.e. the stacking fault energy (SFE). SFE affects many physical phenomena on the micro- and macro-scales, controlling the mode of deformation at both low and high deformation temperature and how a plastically deformed material recrystallizes.

In high SFE fcc alloys, the stacking fault is very narrow, and can be recombined with relative ease, hence climb and cross slip of dislocations are the basic modes of deformation<sup>2</sup>. However, as the SFE decreases, there is an increase in the width of separation of the partial dislocations that reduces the propensity for cross slip and climb, thereby decreasing ductility. Further, deformation twinning can occur more readily in some low SFE alloys as an alternative means of accommodating stress (e.g. in

Cu-Zn brasses, where Zn is found to significantly lower the stacking fault energy of Cu)<sup>3,4</sup>. While there are many other relevant factors such as grain size, SFE has been shown to be a useful metric for predicting and understanding plastic deformation behavior in fcc alloys at low homologous deformation temperatures<sup>5,6</sup>. With respect to their engineering performance, engineering safety factors and the industrial processability of alloys, the ability to predict and compare ductility by fundamental calculations of SFE is a powerful engineering and processing tool for alloy design and development.

Considerable effort has been spent on calculating SFE from first principles in order to predict and confirm experimental results as well as understand the fundamentals of deformation from the atomic level. Furthermore, measurements of SFE are difficult and often inaccurate. Accurate methods for calculating SFE in binary alloys can be extended to aid the development of more complex multicomponent alloys, such as high entropy alloys, which contain five or more elements in close to equiatomic proportions<sup>7</sup>. In addition, the SFE of binary and ternary alloys may provide insights into more complex alloys based on them. Many studies of SFE concern dilute alloys, investigating the effect of individual solute atoms within or near the fault plane<sup>4,8,9</sup>. Ideal methods would work for non-dilute and dilute alloys alike in order to examine the full composition space of alloy systems. While effective medium theories have been used to calculate SFE in non-dilute alloys, an optimal method for calculating SFE by modelling the atomic species explicitly in such systems remains unclear.

The concept of stacking fault energy has been extended to the generalized stacking fault energy (GSFE) curve, which is the energy per unit area of stacking fault formation along a particular direction<sup>10,11</sup>. The curve has two stable energy minima,  $\gamma_{\text{isf}}$  and  $\gamma_{\text{esf}}$ , which are the intrinsic (one layer removed) SFE and extrinsic (one layer

added) SFE, respectively. It also contains the unstable SFE  $\gamma_{\text{usf}}$  and the unstable twin fault energy  $\gamma_{\text{utf}}$  as local maxima, representing the energy barriers to creating an intrinsic stacking fault and an extrinsic stacking fault, respectively. These unstable energies, while experimentally inaccessible, are thought to be important in determining an alloy’s tendency toward slip or twinning<sup>6,12</sup>. The GSFE curve can be extended to include an arbitrary number of consecutive faults in order to examine twin growth<sup>13</sup>.

One commonly used technique to calculate SFE is the axial interaction model (AIM), or the axial next-nearest-neighbor Ising model. The energy of an arbitrary stacking sequence can be expanded based on how it differs from the nominal fcc sequence up to some number of nearest neighbors<sup>14</sup>. This allows one to approximate the SFE as a function of the energies of different stacking sequences. The first-order AIM is simply the difference in energy between hexagonal close-packed (hcp) and fcc, which highlights the idea that a stacking fault is a region of local hcp stacking<sup>15</sup>. Higher-order approximations can be obtained by including more stacking sequences. The third-order AIM includes the double hexagonal close-packed (dhcp) energy in addition to the hcp and fcc energies. Many have found the AIM estimate to be sufficient<sup>16–19</sup> and it is computationally inexpensive, since it does not require modeling stacking faults directly using large supercells. The major disadvantage of this approach is that it can only provide estimates of stable energies  $\gamma_{\text{isf}}$  and  $\gamma_{\text{esf}}$ , so it does not provide any additional information from the GSFE curve.

Obtaining the full GSFE curve requires calculating the energy of a single supercell as half of it is displaced relative to the other. This is straightforward for pure elements, but it presents a challenge for modeling disordered alloys. Two main methods have been employed in the literature to account for disorder in solid solution alloys. The first is the coherent potential approximation (CPA), which approximates the random alloy as a small periodic lattice of a single “effective potential” that is representative of the average electronic characteristics of the alloy stoichiometry<sup>20,21</sup>. This technique has been used to determine GSFE in various binary and more complex systems<sup>3,4,22–25</sup>. The main drawback of CPA is that because chemically identical atoms are treated the same regardless of their local environment, it cannot account for local lattice distortions, which can be important in many non-dilute systems such as high entropy alloys<sup>26,27</sup>.

The other technique of modeling disordered alloys is the use of special quasirandom structures (SQSs). An SQS is a finite-size arrangement of atoms that approximates the target random structure as closely as desired<sup>28</sup>. This is achieved by considering symmetrically equivalent groups of lattice sites (pairs, triplets, etc) and matching—in a finite periodic cell up to a certain interaction distance—the average interactions up to those expected in a perfectly random alloy<sup>29</sup>. Because the different species are modeled explicitly, this accounts for

local lattice effects. However a major disadvantage of SQSs compared to CPA is that the number of atoms, and therefore the supercell geometry, is constrained by the composition. SQSs also must be sufficiently large in order to accurately model the disordered state, increasing computational cost.

While some have shown good agreement between SQS and CPA approaches to calculating bulk properties such as elastic constants and mixing enthalpy<sup>30,31</sup>, there has not been significant comparison of CPA and SQS for calculating GSFE. Since introducing a stacking fault in an SQS breaks the symmetry of the structure and changes the correlations, some kind of averaging is required to ensure that the calculated SFE actually reflects the average of the true alloy. Noting this, Chandran et al. calculated SFE in non-dilute Ni-Co alloys using randomly assigned atomic positions rather than SQSs and averaging over multiple structures<sup>18</sup>. de Jong et al. calculated unstable stacking fault, twin boundary, and surface energies in non-dilute hcp Ti-Al alloys by SQSs by averaging over the choice of fault plane within the supercell<sup>32</sup>. They also used a benchmarking technique to show that the SQSs provided a more accurate result on average than simply assigning positions randomly. This method of planar averaging has not been done for fcc alloys.

In the present study, we use a planar averaging approach to directly calculate GSFE for non-dilute fcc binary alloys in the Ag-Au-Pd system. This system was chosen because it is a model fcc solid solution system with no ordering, and it is known that Ag has one of the lowest SFEs. We investigate how the number of atoms used in the SQS affects the accuracy of SFE predictions and we propose a novel method to evaluate the quality of an SQS for future SFE calculations. We also compare our results to available CPA results and to first- and third-order AIM approximations of  $\gamma_{\text{isf}}$ .

## II. METHODOLOGY

### A. SQS generation

All density functional calculations were performed on special quasirandom structures generated using *mcsqs*, a Monte Carlo-based algorithm that is part of the Alloy-Theoretic Automated toolkit (ATAT)<sup>33,34</sup>. Pair clusters up to 1.8 times the nearest neighbor distance and nearest neighbor triplets were included in the objective function to evaluate the SQSs. This resulted in three pairs, one triplet for fcc; six pairs, three triplets for hcp; and nine pairs, five triplets for dhcp. The objective function used in the *mcsqs* algorithm was the average absolute value of correlation mismatches for the chosen clusters relative to an ideal random solution. Ten independent instances of *mcsqs* were run concurrently, and the resulting SQSs were considered optimized when all ten instances stabilized to the same value of the objective function. Since SQSs are independent of atomic species, we only needed to

generate SQSs for each distinct stoichiometry and size of cell.

### B. Total energy calculations

Total energy calculations were performed using the Vienna Ab initio Simulation Package implementation of density functional theory<sup>35,36</sup>. The lattice parameter for each composition was the ground state lattice parameter determined by fitting the Birch-Murnaghan equation of state<sup>37</sup> to a series of 11 fixed volumes of a 30 atom SQS. The ionic positions were allowed to relax fully. A verification with larger SQSs gave the same ground state lattice parameter to within 0.001 Å. The ground state lattice parameter for each composition was consistently used for all subsequent calculations of larger cells.

A plane wave energy cutoff of 450 eV was used for all calculations. Smearing was performed with the first-order method of Methfessel-Paxton with a smearing parameter of 0.2<sup>38</sup>. Gamma-centered Monkhorst-Pack meshes with about 20,000 k-points per reciprocal atom were used to sample the Brillouin zone for all structures<sup>39</sup>. These settings were found to be sufficient for convergence of total energy to within 1E-4 eV per atom, corresponding to around 1 mJ/m<sup>2</sup> for fault energies.

Projector augmented wave (PAW) potentials were used with the Perdew-Burke-Ernzerhof generalized gradient (PBE-GGA) exchange correlation approximation<sup>40,41</sup>. A quasi-Newton algorithm and automatic real-space projections were used for ionic relaxations, and forces were converged to within 0.02 eV/Å. To obtain accurate final energies, all relaxations were followed by a final static calculation with the linear tetrahedron method on and real-space projections off. A mixture of Blocked Davidson and RMM-DIIS algorithms for electronic minimization was used (ALGO = Fast).

### C. Direct supercell method

Direct calculations of GSFE used SQS supercells with nine (111) layers in perfect fcc stacking. The layers were periodic along  $[01\bar{1}]$  and  $[10\bar{1}]$ . Nine layers were sufficient to isolate faults from their periodic images (calculations with twelve layers did not give significantly different SFE for any pure element in the system). This is consistent with the findings of others<sup>25,42</sup>. Calculations were performed on cells of 90 atoms (10 per layer) and 135 atoms (15 per layer). Figure 1 shows an example of a 90-atom supercell looking along the  $[01\bar{1}]$  direction.

Stacking faults were created using the method of Kibey et al.<sup>13</sup>, in which the top five layers shift along  $[11\bar{2}]$  in two steps to form one intrinsic stacking fault, then the top four layers shift in two steps to form one extrinsic stacking fault. Each shift is accompanied by a small adjustment of the long lattice vector (originally  $[111]$ ) in

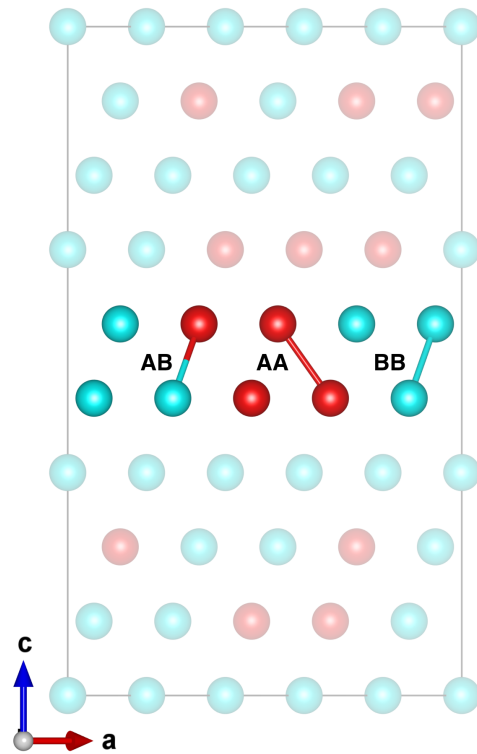


FIG. 1. Isolated set of adjacent layers in a 90-atom A-80% B SQS with examples of the three possible interactions for the interlayer pair cluster shown. Visualization created using VESTA<sup>43</sup>.

order to preserve fcc stacking between periodic cells. The ionic positions of the defect-free cell were fully relaxed. For each shift, the positions of all ions were relaxed only along the long direction. As noted by de Jong et al.<sup>32</sup>, since the choice of layer at which to shear is arbitrary, calculations were performed for each of the nine possible fault planes to produce an average and standard deviation for each fault energy.

### D. Axial interaction model

We calculated the first-order axial interaction model approximation (AIM1), by

$$\gamma_{\text{isf}} \approx 2(E_{\text{hcp}} - E_{\text{fcc}})/A_{111} \quad (1)$$

and the third-order approximation (AIM3), by

$$\gamma_{\text{isf}} \approx (E_{\text{hcp}} + 2E_{\text{dhcp}} - 3E_{\text{fcc}})/A_{111} \quad (2)$$

where  $\gamma_{\text{isf}}$  is intrinsic stacking fault energy,  $E$  is the total energy of each respective stacking sequence, and  $A_{111}$  is the (111) area per atom<sup>14</sup>. As noted by Li et al.<sup>14</sup>, the energies for hcp and dhcp are not the theoretical ground state energies for those structures since they are calculated at the fcc ground state volume per atom with the ideal  $c/a$  ratio. Other AIM variants exist to include

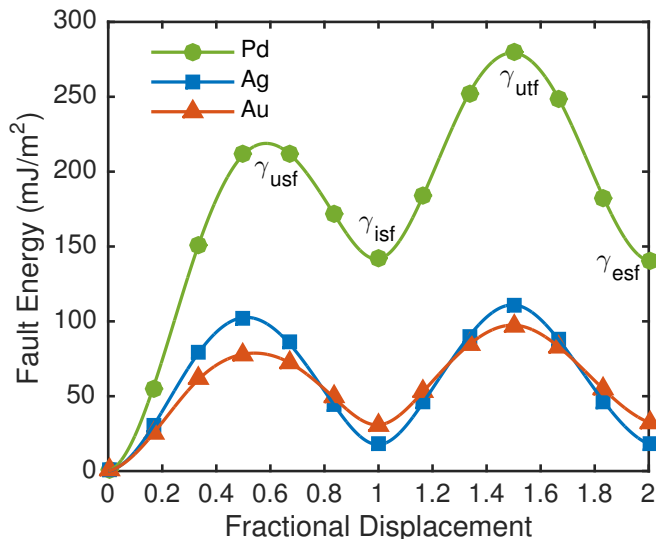


FIG. 2. Generalized stacking fault energy curves for pure elements studied.

relaxation of the interlayer distance as well as interfacial energies between phases, but those are not the focus of this study.

For SFE calculations using the AIM, SQSs of 60 and 80 atoms were used for hcp and dhcp structures, respectively. The ionic positions were allowed to relax fully. The AIM3 calculation is particularly sensitive to the fcc total energy since it enters with a factor of three. We compare using the energy of the 90-atom and 135-atom fcc SQSs from the direct supercell calculations as well as the energy of the 30-atom fcc SQS from the equation of state calculations to estimate the effect of SQS size on the AIM calculation of SFE.

### III. RESULTS AND DISCUSSION

#### A. Pure elements

GSFE curves for pure Ag, Au and Pd are summarized in Table I and shown in Figure 2. The calculated values for each are in agreement with the available first-principles literature.

As others have found,  $\gamma_{\text{usf}}$  occurs near 0.5 for Ag and Au, and somewhere in between a fractional displacement of 0.5 and 0.66 for Pd<sup>46,47</sup>. In order to reduce computational expense,  $\gamma_{\text{usf}}$  for alloys was taken to be at 0.5 for all alloys even though this likely slightly underestimates the energy for the Pd alloys. It appears that  $\gamma_{\text{utf}}$  occurs at around 1.5 for all three elements. In this study, energies for the alloys are calculated at fractional displacements of 0.5, 1.0, 1.5 and 2.0. One could easily calculate more intermediate points on the GSFE curve, albeit at increased computational cost since each data point involves averaging over nine layers.

#### B. Direct supercell method

Figure 3 shows the calculated stacking fault energies using 135-atom SQSs versus composition for Pd-Ag, Pd-Au, and Ag-Au. Since the pure elements are each fcc, within a mean-field approximation we would expect to see a linear average of the elemental energies for each intermediate composition. Deviations from this average indicate that one element has a stronger influence on the SFE when alloyed. It appears that Ag has a stronger effect than Pd on SFE when alloyed, whereas Au has a weaker effect than Pd, as indicated by the curvature of the energies in Figure 3 ab and cd, respectively.

For Pd-Ag, shown in Figure 3 ab and Pd-Au, shown in Figure 3 cd, there is good agreement between the present study and the EMTO-CPA results from Li et al.<sup>4</sup> for the stable SFE. For the unstable energies, they obtained a higher  $\gamma_{\text{usf}}$  and  $\gamma_{\text{utf}}$ , though the qualitative behavior versus the concentration is similar. The unstable energies are about 20 to 50 mJ/m<sup>2</sup> higher for Pd-Ag and about 50 to 60 mJ/m<sup>2</sup> higher for Pd-Au. However for  $\gamma_{\text{usf}}$  in Pd-Ag, the difference is gets smaller with increasing Ag content. Because this discrepancy exists for the pure elements as well as alloys, it is likely not due to differences in the CPA and SQS approaches for modelling alloys.

A possible cause of this discrepancy is that Li et al. relaxed the supercells differently by relaxing the interlayer distance of the first neighbors nearest to the fault plane. We attempted this for pure Ag, Au and Pd but found that it did not yield significantly different SFE values, and in fact resulted in unstable SFE values that were several mJ/m<sup>2</sup> lower than obtained previously. However, without knowing what algorithms were used, it is difficult to compare directly. As shown in Table I, there tends to be much more variation in the literature for unstable SFE than stable SFE, as they are very sensitive to slight differences in methods.

For Ag-Au, for which there is no available literature data, it appears the stable stacking fault energies are close to an average of the pure elements, whereas Ag influences the unstable SFE slightly more than Au. However, the uncertainty is large compared to the differences between adjacent points. Since the different compositions are very close in SFE, this system is near the limit of this method's effectiveness.

Table II lists the stacking fault energies and standard deviations for each binary composition calculated from both 90- and 135-atom SQSs. Presumably using more atoms per layer will always give a more accurate result for SFE since it will be closer to the actual random arrangement. However, there is a tradeoff between accuracy and computational cost. We found that the correlations of a 180-atom SQS were only slightly better than those of a 135-atom SQS and that it would require a 225 atom SQS to perfectly match all of the chosen pair correlations. For these reasons we did not calculate SFE using more than 135 atoms.

In almost all cases, using 135 atoms produces an energy

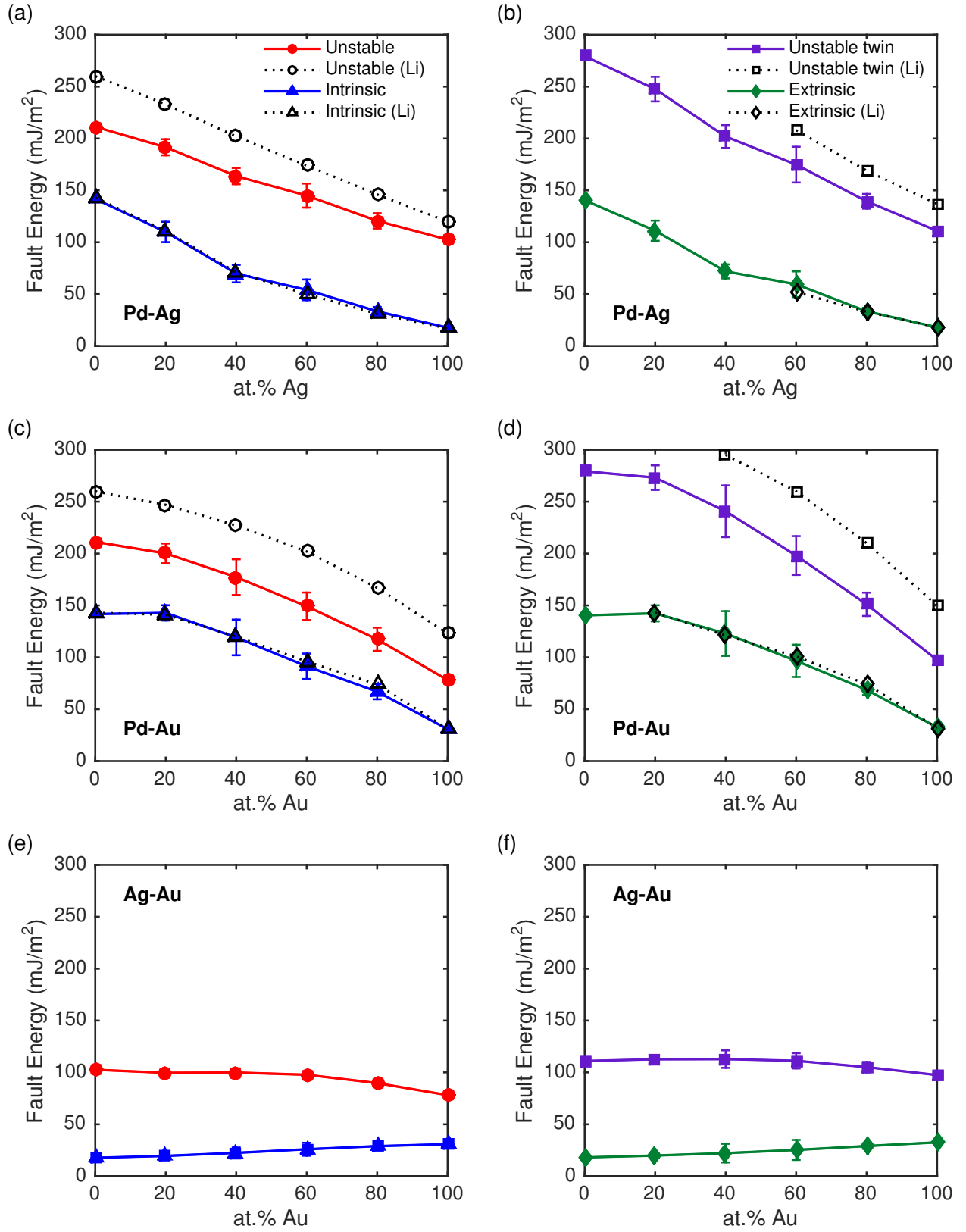


FIG. 3.  $\gamma_{\text{usf}}$  and  $\gamma_{\text{isf}}$ ,  $\gamma_{\text{utf}}$  and  $\gamma_{\text{esf}}$  versus Ag content for Pd-Ag (a, b), versus Au content for Pd-Au (c, d), versus Au content for Ag-Au (e, f). Error bars indicate  $\pm$  one standard deviation. Results are compared to available data from Li et al.<sup>4</sup>

TABLE I. Stable and unstable stacking fault energies for pure elements studied compared to literature values (in parentheses). Lattice parameters  $a_{fcc}$  are in Å and all energies are in mJ/m<sup>2</sup>.

	$a_{fcc}$	$\gamma_{usf}$	$\gamma_{isf}$	$\gamma_{utf}$	$\gamma_{esf}$
Ag	4.147	103 (91 <sup>a</sup> , 111 <sup>b</sup> , 120 <sup>c</sup> , 133 <sup>d</sup> )	18 (16 <sup>a</sup> , 17 <sup>b,c</sup> , 18 <sup>d</sup> )	111 (100 <sup>a</sup> , 137 <sup>c</sup> , 143 <sup>d</sup> )	18 (12 <sup>a</sup> , 18 <sup>c,d</sup> )
Au	4.156	78 (68 <sup>a</sup> , 94 <sup>b</sup> , 123 <sup>c</sup> , 134 <sup>d</sup> )	31 (25 <sup>a</sup> , 27 <sup>b</sup> , 31 <sup>c</sup> , 33 <sup>d</sup> )	97 (79 <sup>a</sup> , 148 <sup>d</sup> , 150 <sup>c</sup> )	33 (27 <sup>a</sup> , 31 <sup>d</sup> , 32 <sup>c</sup> )
Pd	3.940	212 (202 <sup>a</sup> , 215 <sup>b</sup> , 260 <sup>c</sup> , 287 <sup>d</sup> )	142 (122 <sup>b</sup> , 134 <sup>a</sup> , 143 <sup>c</sup> , 168 <sup>d</sup> )	279 (261 <sup>a</sup> , 361 <sup>d</sup> )	140 (129 <sup>a</sup> , 172 <sup>d</sup> )

a 44

b 45

c 4

d 13

TABLE II. Stable and unstable stacking fault energies for Pd-Ag, Pd-Au, and Ag-Au alloys using 90 and 135 atoms  $\pm$  one standard deviation. Italicized energies indicate that using more atoms gave a significantly different energy (one 90-atom standard deviation or more), bolded energies indicate that using more atoms increased the standard deviation. Lattice parameters  $a_{fcc}$  are in Å and all energies are in mJ/m<sup>2</sup>.

	$a_{fcc}$	$\gamma_{usf}$		$\gamma_{isf}$		$\gamma_{utf}$		$\gamma_{esf}$	
		90	135	90	135	90	135	90	135
Pd-20% Ag	3.979	189 $\pm$ 14	192 $\pm$ 8	106 $\pm$ 17	110 $\pm$ 10	245 $\pm$ 20	248 $\pm$ 12	108 $\pm$ 12	111 $\pm$ 10
Pd-40% Ag	4.017	163 $\pm$ 11	164 $\pm$ 8	70 $\pm$ 14	70 $\pm$ 8	200 $\pm$ 18	202 $\pm$ 11	72 $\pm$ 14	72 $\pm$ 7
Pd-60% Ag	4.056	146 $\pm$ 13	145 $\pm$ 12	55 $\pm$ 11	54 $\pm$ 10	<b>177 <math>\pm</math> 15</b>	<b>175 <math>\pm</math> 17</b>	<b>60 <math>\pm</math> 10</b>	<b>59 <math>\pm</math> 12</b>
Pd-80% Ag	4.100	124 $\pm$ 15	121 $\pm$ 7	39 $\pm$ 11	33 $\pm$ 4	149 $\pm$ 18	139 $\pm$ 7	<i>48 <math>\pm</math> 9</i>	<i>33 <math>\pm</math> 3</i>
Pd-20% Au	3.985	198 $\pm$ 17	200 $\pm$ 10	138 $\pm$ 16	143 $\pm$ 7	270 $\pm$ 20	273 $\pm$ 12	139 $\pm$ 13	142 $\pm$ 8
Pd-40% Au	4.028	178 $\pm$ 18	178 $\pm$ 17	120 $\pm$ 18	119 $\pm$ 17	<b>243 <math>\pm</math> 22</b>	<b>241 <math>\pm</math> 25</b>	<b>126 <math>\pm</math> 16</b>	<b>123 <math>\pm</math> 22</b>
Pd-60% Au	4.069	153 $\pm$ 18	149 $\pm$ 13	98 $\pm$ 16	91 $\pm$ 12	210 $\pm$ 24	198 $\pm$ 19	<b>109 <math>\pm</math> 13</b>	<b>97 <math>\pm</math> 16</b>
Pd-80% Au	4.111	118 $\pm$ 25	117 $\pm$ 11	70 $\pm$ 19	67 $\pm$ 7	159 $\pm$ 31	151 $\pm$ 11	77 $\pm$ 15	69 $\pm$ 5
Ag-20% Au	4.147	<i>103 <math>\pm</math> 2</i>	<i>100 <math>\pm</math> 2</i>	<i>23 <math>\pm</math> 3</i>	<i>20 <math>\pm</math> 2</i>	112 $\pm$ 2	113 $\pm$ 2	<i>24 <math>\pm</math> 3</i>	<i>20 <math>\pm</math> 3</i>
Ag-40% Au	4.148	103 $\pm$ 4	100 $\pm$ 4	<i>29 <math>\pm</math> 5</i>	<i>22 <math>\pm</math> 5</i>	<b>117 <math>\pm</math> 6</b>	<b>113 <math>\pm</math> 8</b>	<b>33 <math>\pm</math> 6</b>	<b>22 <math>\pm</math> 9</b>
Ag-60% Au	4.149	98 $\pm$ 5	98 $\pm$ 3	<b>31 <math>\pm</math> 5</b>	<b>26 <math>\pm</math> 6</b>	113 $\pm$ 7	111 $\pm$ 7	<b>34 <math>\pm</math> 5</b>	<b>25 <math>\pm</math> 10</b>
Ag-80% Au	4.153	89 $\pm$ 7	90 $\pm$ 3	29 $\pm$ 4	29 $\pm$ 2	102 $\pm$ 8	105 $\pm$ 5	29 $\pm$ 4	29 $\pm$ 3

that is within one standard deviation of the energy found using 90 atoms. The uncertainty also tends to decrease or remain constant when increasing to 135, with several exceptions where the error actually increased. Since the same SQSs were used for each stoichiometry, it is interesting that the different binary systems do not display quite the same trends in going from 90 to 135 atoms. For instance there is a large jump of 15 mJ/m<sup>2</sup> for  $\gamma_{esf}$  of Pd-80% Ag, but a smaller jump of 8 mJ/m<sup>2</sup> for  $\gamma_{esf}$  of Pd-80% Au, which itself is larger. Significant jumps from 90 to 135 atoms occur most for  $\gamma_{esf}$ . This could be due to the fact that it is the result of two shifts of consecutive layers, so the variation in the structures of both sets of layers is more pronounced in the final energy. Although it is not certain the SFE values stabilize at 135 atoms, we are reassured that 135-atom results agree well with Li et al.

Examining the SQSs more closely reveals why the uncertainty may increase in some cases between a 90- to 135-atom cell size. Since we used the same SQSs for each binary system, we only needed to analyze the generic A-80% B and A-60% B SQSs for 90 and 135 atoms. ATAT

was used to isolate pairs of adjacent layers within each defect-free SQS and extract only the point and nearest neighbor pair correlations between the selected layers. The point correlation average  $B$  is simply the concentration of B atoms within the chosen layers. For the nearest neighbor pair correlations, we extracted the *inter-layer* correlation averages—denoted  $AA$ ,  $BB$ , and  $AB$ —from the intralayer correlations. In the perfectly random structure, these would average to the square of the concentration of A, the square of the concentration of B, and the product of the concentrations of A and B, respectively. Figure 1 illustrates the method of isolating adjacent layers.

For each SQS, the interlayer correlations were calculated for each pair of adjacent layers and averaged, similar to how the SFE calculations are averaged over each layer. The results are shown in Table III. In each case, the average concentration  $B$  is equal to the overall concentration of B in the SQS, which will always be true. But the variation shows that each layer does not have the exact same composition. For A-80% B, increasing the number of atoms does not change any of the average pair

TABLE III. Interlayer correlations averaged over each set of adjacent layers within each SQS ( $\pm$  one standard deviation).

% B	at.	$B_{\text{avg}}$	$AA_{\text{avg}}$	$BB_{\text{avg}}$	$AB_{\text{avg}}$
80	90	$0.80 \pm 0.11$	$0.04 \pm 0.05$	$0.64 \pm 0.19$	$0.16 \pm 0.08$
80	135	$0.80 \pm 0.06$	$0.04 \pm 0.04$	$0.64 \pm 0.09$	$0.16 \pm 0.03$
60	90	$0.60 \pm 0.11$	$0.17 \pm 0.11$	$0.37 \pm 0.11$	$0.23 \pm 0.03$
60	135	$0.60 \pm 0.07$	$0.15 \pm 0.07$	$0.35 \pm 0.10$	$0.25 \pm 0.05$

correlations, but their standard deviations all decrease, as we would expect with more atoms interacting between each layer. For A-60% B, however, increasing the number of atoms gives slightly different average correlations for  $AA$ ,  $BB$ , and  $AB$ . In addition, the standard deviation of the  $AB$  average actually increases. This may explain why in Table II, the only increase in uncertainty in using the 135-atom cell was for the 40/60 and 60/40 compositions. Presumably the A-B interactions are energetically important in the SFE calculation, so an increase in the AB uncertainty is reflected in the average SFE. We also found that the uncertainty in all intralayer correlations decreased from 90 to 135 atoms.

These results indicate that a more tailored method of SQS generation may be required for improved average SFE calculations. For instance a novel objective function that takes into account the overall correlations as well as the correlations between sets of layers could help pre-screen SQSs for improved SFE calculations.

### C. AIM method

Table IV lists the results of the first- and third-order AIM estimates for  $\gamma_{\text{isf}}$  in the pure elements. While both AIM1 and AIM3 show good agreement for Ag and Au, AIM3 overestimates  $\gamma_{\text{isf}}$  by almost 10% for Pd, indicating this expansion may not be sufficient for Pd. The discrepancy for Pd could be due to fixing the interlayer distance of the dhcp and hcp phases, since allowing them to relax would likely yield a lower energy. Using higher-order AIM expansions with more stacking sequences could also provide a better approximation. Others have also observed the stacking fault energy contains an hcp-fcc interfacial energy which the AIM method does not account for, adding another layer of discrepancy between the AIM method and direct supercell methods<sup>14</sup>. This may account for AIM underestimating the SFE in some cases.

Table V contains the results of AIM estimates for the three binary alloy systems studied. Applied to these systems, AIM3 (using 135 atom SQSs for fcc) estimates  $\gamma_{\text{isf}}$  as calculated directly using 135 atoms to within 10% in all but one case. However using 30- and 90-atom cells for the fcc energy introduces significant variation which is not always monotonic. There are several compositions for which the AIM3 values for 30 and 135 atoms are close

TABLE IV. First- and third-order AIM results for pure elements compared to  $\gamma_{\text{isf}}$  as calculated directly. All energies are in  $\text{mJ}/\text{m}^2$ .

	AIM1	AIM3	$\gamma_{\text{isf}}$
Ag	17	17	18
Au	32	31	31
Pd	170	155	142

TABLE V. First- and third-order AIM results using 30, 90 and 135 atoms for fcc compared to direct supercell calculations using 135 atoms. All energies are in  $\text{mJ}/\text{m}^2$ .

	AIM1			AIM3			$\gamma_{\text{isf}}$
	30	90	135	30	90	135	
Pd-20% Ag	107	118	106	108	125	106	110
Pd-40% Ag	69	76	74	65	75	72	70
Pd-60% Ag	49	47	51	43	40	46	54
Pd-80% Ag	30	31	31	33	34	35	33
Pd-20% Au	148	149	149	145	145	146	143
Pd-40% Au	109	118	122	103	116	121	119
Pd-60% Au	84	86	92	72	75	84	91
Pd-80% Au	65	58	67	65	55	69	67
Ag-20% Au	22	20	23	22	23	21	20
Ag-40% Au	16	22	24	26	24	19	22
Ag-60% Au	26	29	28	25	28	26	26
Ag-80% Au	31	31	31	29	29	30	29

but the 90-atom value is significantly different. From this we conclude that the AIM method is quite sensitive to the specific structure used. We did not use different hcp and dhcp structures, which would likely introduce additional uncertainty. However, averaging over multiple SQSs with similar correlations can provide a better estimate while still limiting computational cost, as others have shown<sup>18</sup>.

### D. Universal scaling law

Jin et al. proposed a “universal scaling law” for the ratio of  $\gamma_{\text{isf}}$  to  $\gamma_{\text{usf}}$  and of  $\gamma_{\text{utf}}$  to  $\gamma_{\text{usf}}$

$$\frac{\gamma_{\text{utf}}}{\gamma_{\text{usf}}} \approx 1 + \frac{\gamma_{\text{isf}}}{2\gamma_{\text{usf}}}. \quad (3)$$

They showed this relationship to hold for when the interaction of the consecutive stacking faults is negligible, which they found to be true of many fcc elements, with Pt as an exception<sup>44</sup>. This is a useful result because common measures of propensity for twinning during deformation rely on the ratio  $\gamma_{\text{utf}}/\gamma_{\text{usf}}$ , so taking advantage of this scaling law could reduce computational expense<sup>12</sup>.

As shown in Figure 4, we find that the law holds well for all alloys considered. The shift between our results and those from Li et al. is due to the discrepancy in

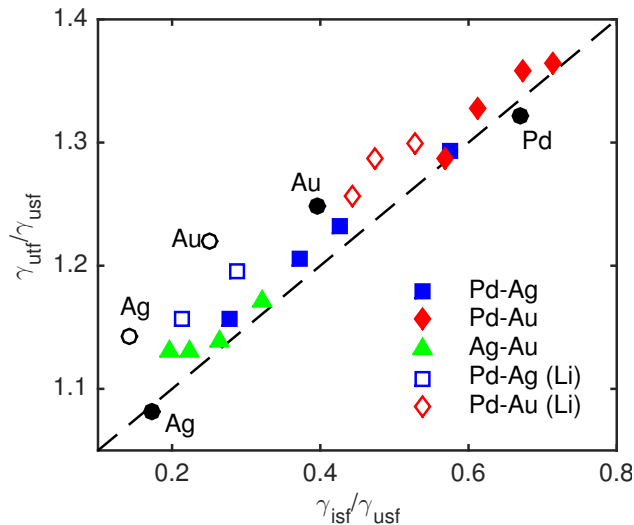


FIG. 4.  $\gamma_{ustf}/\gamma_{usf}$  versus  $\gamma_{isf}/\gamma_{usf}$  for all pure elements and binary compositions studied and those from Li et al.<sup>4</sup>.

the unstable SFE that was noted previously. Our results follow the scaling law more closely, particularly for Ag and Pd-Ag.

#### IV. CONCLUSIONS

In this study, we have examined a direct method for calculating SFE in non-dilute Pd-Ag, Pd-Au, and Ag-Au alloys by averaging over all possible fault planes within

a single SQS. Our results are in good agreement with available CPA literature for stable SFE, however there is a discrepancy in the unstable SFE which could be due to slight differences in methods. We found that using 135 atoms versus 90 atoms tends to reduce the uncertainty of the calculated energy, except for some cases which we attribute to an increase in the variation of certain interlayer interactions. This result in particular suggests that a new strategy of pre-screening SQSs based on not just the overall correlations but correlations between layers may provide a way to improve these kinds of SFE calculations. We also found that the AIM method estimates the direct supercell method within 10% in almost all cases, but can be quite sensitive to the particular structure. We expect these results will be useful in choosing the best methods to calculate SFE of novel alloys.

#### ACKNOWLEDGMENTS

We acknowledge the financial support of NSF grant OISE-1261525 and the Laspa Fellowship at Harvey Mudd College. We appreciate the assistance and support of Caitlin Healy and Paul Munroe in the School of Materials Science and Engineering at UNSW. A.P.J. was supported by the University of California President's Post-doctoral Fellowship. Part of this work was performed under the auspices of the U.S. Department of Energy by Lawrence Livermore National Laboratory under Contract DE-AC52-07NA27344. This work used the Extreme Science and Engineering Discovery Environment (XSEDE), which is supported by National Science Foundation grant number ACI-1053575.

- 
- <sup>1</sup> D. Hull and D. J. Bacon, *Introduction to dislocations* (Butterworth-Heinemann, 2001).
  - <sup>2</sup> F. Humphreys and M. Hatherly, *Recrystallization and related annealing phenomena* (Elsevier, 2004).
  - <sup>3</sup> A. Zaddach, C. Niu, C. Koch, and D. Irving, *Jom* **65**, 1780 (2013).
  - <sup>4</sup> W. Li, S. Lu, Q.-M. Hu, S. K. Kwon, B. Johansson, and L. Vitos, *Journal of Physics: Condensed Matter* **26**, 265005 (2014).
  - <sup>5</sup> E. El-Danaf, S. R. Kalidindi, and R. D. Doherty, *Metalurgical and Materials Transactions A* **30**, 1223 (1999).
  - <sup>6</sup> M. Jo, Y. M. Koo, B.-J. Lee, B. Johansson, L. Vitos, and S. K. Kwon, *Proceedings of the National Academy of Sciences* **111**, 6560 (2014).
  - <sup>7</sup> J.-W. Yeh, S.-K. Chen, S.-J. Lin, J.-Y. Gan, T.-S. Chin, T.-T. Shun, C.-H. Tsau, and S.-Y. Chang, *Advanced Engineering Materials* **6**, 299 (2004).
  - <sup>8</sup> S. A. Kibey, L.-L. Wang, J. B. Liu, H. T. Johnson, H. Sehitoglu, and D. D. Johnson, *Physical Review B* **79**, 214202 (2009).
  - <sup>9</sup> S. Shang, Y. Wang, Y. Du, M. A. Tschopp, and Z.-K. Liu, *Computational Materials Science* **91**, 50 (2014).
  - <sup>10</sup> V. Vitek, *Philosophical Magazine* **18**, 773 (1968).
  - <sup>11</sup> V. Vitek, *Cryst. Lattice Defects* **5**, 1 (1974).
  - <sup>12</sup> N. Bernstein and E. B. Tadmor, *Physical Review B* **69**, 094116 (2004).
  - <sup>13</sup> S. Kibey, J.-B. Liu, D. Johnson, and H. Sehitoglu, *Acta Materialia* **55**, 6843 (2007).
  - <sup>14</sup> R. Li, S. Lu, D. Kim, S. Schönecker, J. Zhao, S. K. Kwon, and L. Vitos, *Journal of Physics: Condensed Matter* **28**, 395001 (2016).
  - <sup>15</sup> K. Ishida, *physica status solidi (a)* **36**, 717 (1976).
  - <sup>16</sup> L. Vitos, J.-O. Nilsson, and B. Johansson, *Acta Materialia* **54**, 3821 (2006).
  - <sup>17</sup> A. Abbasi, A. Dick, T. Hickel, and J. Neugebauer, *Acta Materialia* **59**, 3041 (2011).
  - <sup>18</sup> M. Chandran and S. Sondhi, *Journal of Applied Physics* **109**, 103525 (2011).
  - <sup>19</sup> S. Lu, Q.-M. Hu, B. Johansson, and L. Vitos, *Acta Materialia* **59**, 5728 (2011).
  - <sup>20</sup> P. Soven, *Phys. Rev.* **156**, 809 (1967).
  - <sup>21</sup> L. Vitos, I. A. Abrikosov, and B. Johansson, *Physical Review Letters* **87**, 156401 (2001).
  - <sup>22</sup> S. Crampin, K. Hampel, D. Vvedensky, and J. MacLaren, *Journal of Materials Research* **5**, 2107 (1990).

- <sup>23</sup> J. M. MacLaren, A. Gonis, and G. Schadler, *Physical Review B* **45**, 14392 (1992).
- <sup>24</sup> T. Schulthess, P. Turchi, A. Gonis, and T.-G. Nieh, *Acta materialia* **46**, 2215 (1998).
- <sup>25</sup> S. Huang, W. Li, S. Lu, F. Tian, J. Shen, E. Holmström, and L. Vitos, *Scripta Materialia* **108**, 44 (2015).
- <sup>26</sup> W. Guo, W. Dmowski, J.-Y. Noh, P. Rack, P. K. Liaw, and T. Egami, *Metallurgical and Materials Transactions A* **44**, 1994 (2013).
- <sup>27</sup> Y. Zhang, T. T. Zuo, Z. Tang, M. C. Gao, K. A. Dahmen, P. K. Liaw, and Z. P. Lu, *Progress in Materials Science* **61**, 1 (2014).
- <sup>28</sup> A. Zunger, S. H. Wei, L. G. Ferreira, and J. E. Bernard, *Physical Review Letters* **65**, 353 (1990).
- <sup>29</sup> A. van de Walle, M. Asta, and G. Ceder, *CALPHAD* **26**, 539 (2002).
- <sup>30</sup> L.-Y. Tian, Q.-M. Hu, R. Yang, J. Zhao, B. Johansson, and L. Vitos, *Journal of Physics: Condensed Matter* **27**, 315702 (2015).
- <sup>31</sup> P. Olsson, I. A. Abrikosov, and J. Wallenius, *Physical Review B* **73**, 104416 (2006).
- <sup>32</sup> M. de Jong, L. Qi, D. L. Olmsted, A. van de Walle, and M. Asta, *Physical Review B* **93**, 094101 (2016).
- <sup>33</sup> A. van de Walle and G. Ceder, *Journal of Phase Equilibria* **23**, 348 (2002).
- <sup>34</sup> A. van de Walle, P. Tiwary, M. de Jong, D. Olmsted, M. Asta, A. D. D. Shin, Y. Wang, L.-Q. Chen, and Z.-K. Liu, *CALPHAD* **42**, 13 (2013).
- <sup>35</sup> G. Kresse and J. Furthmüller, *Comput. Mater. Sci.* **6**, 15 (1996).
- <sup>36</sup> G. Kresse and J. Furthmüller, *Physical review B* **54**, 11169 (1996).
- <sup>37</sup> F. Birch, *Phys. Rev.* **71**, 809 (1947).
- <sup>38</sup> M. Methfessel and A. T. Paxton, *Physical Review B* **40**, 3616 (1989).
- <sup>39</sup> H. J. Monkhorst and J. D. Pack, *Physical review B* **13**, 5188 (1976).
- <sup>40</sup> G. Kresse and D. Joubert, *Physical Review B* **59**, 1758 (1999).
- <sup>41</sup> J. P. Perdew, K. Burke, and M. Ernzerhof, *Phys. Rev. Lett.* **77**, 3865 (1996).
- <sup>42</sup> S. Kibey, J. Liu, D. D. Johnson, and H. Sehitoglu, *Applied physics letters* **89** (2006).
- <sup>43</sup> K. Momma and F. Izumi, *Journal of Applied Crystallography* **41**, 653 (2008).
- <sup>44</sup> Z. Jin, S. Dunham, H. Gleiter, H. Hahn, and P. Gumbsch, *Scripta Materialia* **64**, 605 (2011).
- <sup>45</sup> X.-Z. Wu, R. Wang, S.-F. Wang, and Q.-Y. Wei, *Applied Surface Science* **256**, 6345 (2010).
- <sup>46</sup> M. J. Mehl, D. A. Papaconstantopoulos, N. Kioussis, and M. Herbranson, *Physical Review B* **61**, 4894 (2000).
- <sup>47</sup> A. Hunter, R. Zhang, and I. Beyerlein, *Journal of Applied Physics* **115**, 134314 (2014).